Current Biology 17, 2003–2012, December 4, 2007 ©2007 Elsevier Ltd All rights reserved DOI 10.1016/j.cub.2007.10.066

Article

Mapping of Meiotic Single-Stranded DNA Reveals Double-Strand-Break Hotspots near Centromeres and Telomeres

Hannah G. Blitzblau,[1] George W. Bell,[2] Joseph Rodriguez,[2] Stephen P. Bell,[1] and Andreas Hochwagen[2,*]
[1]Department of Biology
Howard Hughes Medical Institute and
Massachusetts Institute of Technology
31 Ames Street
Cambridge, Massachusetts 02139
[2]Whitehead Institute for Biomedical Research
9 Cambridge Center
Cambridge, Massachusetts 02142

Summary

Background: Every chromosome requires at least one crossover to be faithfully segregated during meiosis. At least two levels of regulation govern crossover distribution: where the initiating DNA double-strand breaks (DSBs) occur and whether those DSBs are repaired as crossovers.
Results: We mapped meiotic DSBs in budding yeast by identifying sites of DSB-associated single-stranded DNA (ssDNA) accumulation. These analyses revealed substantial DSB activity in pericentrometric regions, in which crossover formation is largely absent. Our data suggest that centromeric suppression of recombination occurs at the level of break repair rather than DSB formation. Additionally, we found an enrichment of DSBs within a ~100 kb region near the ends of all chromosomes. Introduction of new telomeres was sufficient for inducing large ectopic regions of increased DSB formation, thereby revealing a remarkable long-range effect of telomeres on DSB formation. The concentration of DSBs close to chromosome ends increases the relative DSB density on small chromosomes, providing an interference-independent mechanism that ensures that all chromosomes receive at least one crossover per homolog pair.
Conclusions: Together, our results indicate that selective DSB repair accounts for crossover suppression near centromeres and suggest a simple telomere-guided mechanism that ensures sufficient DSB activity on all chromosomes.

Introduction

During gametogenesis, a diploid progenitor cell undergoes two distinct nuclear divisions to produce four haploid gametes; in meiosis I, homologous chromosomes are segregated, and in meiosis II, sister chromatids are partitioned. The proper segregation of homologous chromosomes requires the establishment of a physical connection between each homolog pair. In most organisms, this linkage takes the form of a crossover, a reciprocal exchange of DNA strands between homologs [1, 2]. Failure to form stable crossovers results in chromosome nondisjunction, infertility, and birth defects.

Crossovers are the product of homolog-directed repair of meiotic DSBs. Breaks are formed by the topoisomerase-related enzyme Spo11 [3, 4], which becomes covalently linked to the DNA during the reaction. Removal of Spo11 from DNA ends allows 5′-strand resection [5]. The resulting ssDNA forms the substrate for subsequent strand invasion, which is catalyzed by the two recA homologs Rad51 and Dmc1. Approximately half of the strand-invasion reactions are further processed into double Holliday junctions and crossovers [6, 7].

The limiting number of crossovers per meiosis requires strict regulation of crossover formation and distribution. Two mechanisms are thought to ensure that even small chromosomes receive at least one crossover [8, 9]. First, small chromosomes have a higher DSB density than large chromosomes, thereby increasing the chances that one DSB will be repaired as a crossover [10]. Second, a phenomenon called crossover interference prevents the formation of new crossovers near existing crossovers to ensure optimally spaced crossover distribution along chromosomes [2]. In addition, crossovers are prevented in regions in which they would be deleterious to the cell. Crossovers are suppressed near centromeres, where they would interfere with meiotic chromosome segregation [11, 12]. Similarly, crossovers are reduced in the vicinity of the repetitive DNA at the telomeres [13] and in the rDNA [14], where they could lead to interactions between nonhomologous chromosomes and loss of rDNA repeats, respectively.

Crossover distribution is governed to a large extent by the initial placement of DSBs [8, 9]. In budding yeast, much of our understanding of where DSBs form stems from the analysis of *rad50S*-type mutants (*rad50S*, *mre11S*, and *com1/sae2*Δ), in which meiotic DSBs do not get repaired and Spo11 remains covalently attached to the DNA ends [4]. Studies of individual loci showed that DSBs form preferentially at so-called hotspots, the majority of which are located in intergenic regions containing promoters [15, 16]. In addition, genome-wide analysis of Spo11 localization revealed hot and cold regions of DSB formation and showed specific depletion of DSB hotspots near telomeres, centromeres, and the rDNA [10, 16–19]. However, because *rad50S*-type mutations have been shown to change the rate of DSB formation at some loci [20–22], existing DSB maps might not accurately reflect the distribution of DSBs in wild-type cells.

We have developed an alternative method to localize DSB hotpots by detecting the ssDNA intermediate that surrounds each DSB site. Analysis of sites of ssDNA accumulation in meiosis confirmed that DSBs occur predominantly in promoters and are enriched near highly expressed genes. In addition, consistent with genetic data, high levels of DSBs were detected ≥ ~20 kb

*Correspondence: andi@wi.mit.edu

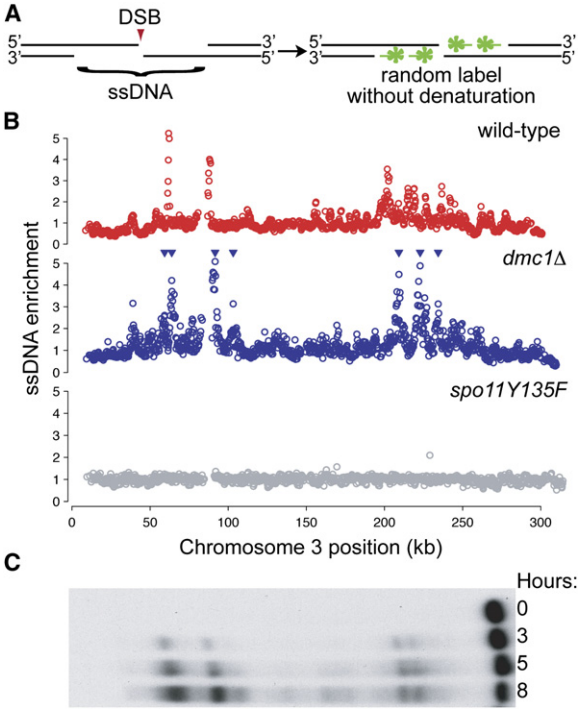

Figure 1. Meiotic ssDNA Profiles

Wild-type (NKY1551), *dmc1*Δ (NKY1455), and *spo11-Y135F* (A10914) cultures were induced to undergo synchronous meiosis. As shown in (A), ssDNA, produced by 5′ to 3′ strand resection at DSBs, was specifically labeled by random priming without a denaturation step. For (B), premeiotic control samples were harvested at 0 hr, and meiotic samples were harvested after 3 hr (NKY1551, A10914) or 5 hr (NKY1455). ssDNA was isolated, labeled, and hybridized to high-density tiled microarrays. The fold enrichment of ssDNA in the meiotic sample over the control sample was calculated for each feature on the array. The average signal from the two independent experiments was plotted versus chromosome position for each feature on chromosome III for wild-type (red), *dmc1*Δ (blue), and *spo11-Y135F* (gray) strains (all chromosomes are shown in Figure S1). Statistically significant DSB sites for *dmc1*Δ are indicated by inverted triangles. For (C), *dmc1*Δ (NKY1455) cells were collected at the indicated time points, and chromosome III was analyzed by pulsed-field gel electrophoresis and Southern blotting with the telomere-proximal *YCL60c* probe [16].

from chromosome ends. Remarkably, we discovered strong DSB hotspots close to centromeres, indicating that the repression of recombination in these regions must occur at the level of DSB repair. Finally, we found that telomeres induce ~100 kb regions of increased DSB formation close to the ends of all chromosomes, suggesting a simple mechanism that distributes DSB activity to chromosomes of all sizes.

Results

Labeling of ssDNA Reveals DSB Sites

We mapped meiotic DSB hotspots by detection of ssDNA, a direct metabolite of DSBs [5, 23] (Figure 1A). Because of its distinct chemical properties, ssDNA can be specifically purified and labeled for microarray analysis [24]. Approximately 600 nucleotides of ssDNA are typically exposed on either side of a meiotic DSB in wild-type cells [5]. This number is increased in *dmc1* mutant cells, which are unable to repair DSBs and arrest with long tracts of ssDNA [25]. Therefore, for our initial analysis, we chose a wild-type SK1 strain, as well as an isogenic *dmc1*Δ mutant strain. Both strains were induced to undergo synchronous meiosis, and total genomic DNA was isolated. ssDNA was enriched and fluorescently labeled. Labeled probes from cells in meiotic prophase and a control population that had not begun DSB formation were cohybridized to a high-density tiled microarray (~300 bp between array features). Plotting the meiotic ssDNA signal versus chromosomal position revealed a reproducible profile of ssDNA enrichment at specific chromosomal loci in both wild-type and *dmc1*Δ strains (Figure 1B and Figure S1 in the Supplemental Data available online). To ensure that the ssDNA signal we detected was due to DSBs induced by Spo11 and not the result of DNA replication or spontaneous DNA damage repair, we performed the same experiment with *spo11-Y135F*, a catalytic mutant of *SPO11*, that is unable to form meiotic DSBs [3]. We observed no sites of significant ssDNA enrichment in the *spo11Y135F* strain (Figure 1B and Figure S1). Therefore, this method specifically detects Spo11-dependent meiotic DSBs.

Consistent with a large body of genetic data, we observed DSBs across most of the genome. We used several approaches to validate the DSB sites predicted by our method. First, ssDNA arrays faithfully reproduced the overall DSB profile of chromosome III as detected by pulsed-field gel electrophoresis and Southern blotting (Figure 1C). We observed that peak height corresponded to signal intensity of hotspots on the Southern blot, indicating that ssDNA signal reflects hotspot activity. Second, we detected all of the well-characterized hotspots that have previously been confirmed by Southern blotting, including *ARG4*, *DED81*, *CYS3*, *HIS2*, *YCR047C*, *CDC19*, and *HIS4LEU2* [8], as well as the majority of hotspots and cold regions directly tested in other genome-wide studies [10, 17]. To further support our results, we analyzed several predicted pericentromeric and telomere proximal hotspots by Southern blotting. In all cases tested, ssDNA profiles were excellent predictors of DSB sites in both wild-type and *dmc1*Δ cells (see below and data not shown). We also confirmed the absence of any measurable hotspot signal in the cold regions surrounding the rDNA array on chromosome XII (*YLR151C–YLR154C* and *YLR163C–YLR176C*; data not shown) [17, 19]. A similar method of ssDNA enrichment was independently developed by Buhler et al., and comparable results were observed [26].

We chose to use the *dmc1*Δ profile for quantitative analysis of DSB distribution because, although ssDNA profiles of wild-type and *dmc1*Δ strains displayed high overall similarity (Figure 1 and Figure S1), the *dmc1*Δ profile exhibited a substantially better signal-to-noise ratio. We believe that this difference in signal is predominantly a consequence of ongoing repair in wild-type cells. Because of the limited synchrony of meiotic cultures, as well as overlap in the timing of meiotic DSB formation and repair [7], some DSBs might already be repaired in wild-type cells while others have yet to form. By contrast, no repair occurs in *dmc1*Δ mutant cells [27]. Furthermore, other recombinases did not contribute *DMC1*-independent repair activity because profiles of *dmc1*Δ *rad51*Δ and *rad52*Δ mutants were nearly

identical to those of *dmc1*Δ (data not shown). Thus, unlike wild-type cells, the *dmc1*Δ mutation probably permits quantitative detection of cumulative DSB formation across the genome.

To search for determinants of hotspot activity, we focused on the most active DSB hotspots because both ssDNA profiles and Southern analysis indicated that the majority of DSB activity occurs at these sites. Multiple contiguous points were enriched above background at each peak, consistent with the density of our array and length of ssDNA exposed in the *dmc1*Δ mutant cells. Therefore, we defined a hotspot as a cluster of >3 adjacent sites that were significantly enriched in at least two individual experiments. By these criteria, we identified 258 hotspots in the *dmc1*Δ strain that we used for subsequent study (blue triangles; Figure 1A, Figure S1, and Table S2).

Hotspots Mapped by ssDNA versus Spo11 Localization

We initially compared the hotspots identified by our ssDNA profiles to hotspots mapped by Spo11 localization analysis (ChIP) in *rad50S* or *sae2*Δ mutants [10, 17]. Of the 258 hotspots detected by ssDNA enrichment in the *dmc1*Δ strain, we found that only 89 overlapped with the 177 DSB sites described by Gerton, et al. [10] and 130 overlapped with the 585 described by Borde, et al. [17]. To eliminate many of the experimental variables that could account for these discrepancies, we mapped sites of Spo11 binding in a *rad50S* SK1 strain on high-density arrays by directly labeling the immunoprecipitated chromatin without amplification (Figure S1). By using the same criteria for hotspot identification as in our ssDNA analysis, we identified 232 significant sites of Spo11 attachment across the genome. Comparison of the DSBs identified by ssDNA enrichment and Spo11 binding in this study revealed 123 loci (~50%) present in both data sets. In addition, we noted that the relative peak heights varied greatly at hotspots that were identified by both ssDNA and Spo11 ChIP. This suggests that the incomplete correspondence between hotspots identified by ssDNA enrichment and Spo11 ChIP was predominantly not a consequence of strain background, array densities, or data analysis.

Previous reports suggested that *rad50S*-type mutations alter DSB frequencies in some parts of the genome [20–22]. To test whether the observed differences between DSB hotspots mapped by ssDNA enrichment and Spo11 ChIP are a consequence of altered DSB distribution between *dmc1*Δ and *rad50S* mutants, we selected several hotspots and analyzed DSB formation in both mutants by Southern blotting. The well-characterized *YCR047C* hotspot was detected by ssDNA mapping and Spo11 ChIP and was equally active in *dmc1*Δ and *rad50S* mutants (Figure 2A). In contrast, several other hotspots close to the telomere of chromosome XVI (*YPL274W* and *YPL221W*; Figure 2A) and in pericentromeric regions (*CEN2*, *CEN4*, and *CEN15*; see below) displayed markedly reduced or undetectable activity in *rad50S* mutants. Altered DSB activity was also apparent by pulsed-field gel electrophoresis and Southern blotting of chromosomes VIII (Figure 2B) and III (Figure S2). Finally, in *rad50S* mutants, a higher fraction of chromosomes remained unbroken, suggesting that overall

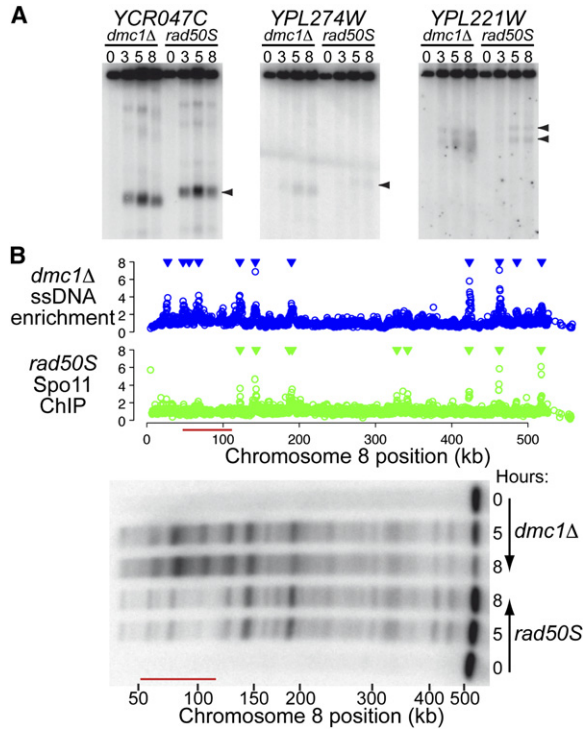

Figure 2. DSB Hotspots in *dmc1*Δ and *rad50S*

*dmc1*Δ (NKY1455) and *rad50S* (A11675) cells were induced to undergo meiosis, and samples were collected at the indicated time points. In (A), genomic DNA was digested and analyzed by Southern blotting. The following restriction enzymes and probes (SGD coordinates) were used: *YCR047C*, HindIII, III:209,361-210,030 [7]; *YPL274W*, PstI/XhoI, XVI:20,281-21,012; and *YPL221W*, XbaI, XVI:128,661-129,550. Black arrowheads indicate major DSB sites. For (B), hotspot distribution on chromosome VIII as determined by ssDNA analysis (top panels) and by pulsed-field gel electrophoresis and Southern blotting (bottom panel). For Southern blotting, a probe close to the left telomere was used (SGD coordinates): VIII:23,768-25,407. Red line indicates region of decreased DSB activity in *rad50S* mutant.

levels of DSB formation might be reduced (Figure 2B and Figure S2). Similar data were obtained by Buhler et al. [26]. We conclude that DSB hotspots are utilized differently in *rad50S* and *dmc1*Δ strains.

DSBs Are Enriched in Promoters of Active Genes

We next examined where breaks occurred with regard to gene-coding regions. Fine-scale mapping of DSBs indicated that they are frequently located in the promoters of one or more adjacent genes within a hotspot [9, 15, 16]. The peaks of ssDNA enrichment we observed had a mean width of 2.6 kb per hotspot and typically overlapped multiple genes. This was expected given ssDNA tract lengths of >1 kb in a *dmc1*Δ mutant [25]. Although our method does not have the resolution to detect individual break points within a hotspot, we employed multiple statistical approaches to reveal trends in DSB site selection. First, assuming that the peak of ssDNA enrichment at each hotspot was located close to the most common break site, we confirmed that DSBs occurred preferentially in promoters. In particular, peaks were located in divergent promoters three times more frequently than expected, whereas they were

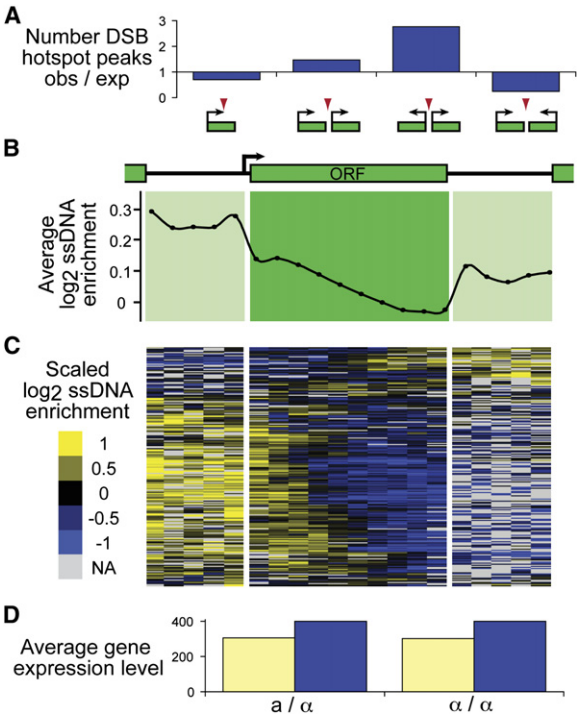

Figure 3. DSBs Are Enriched in Promoters of Active Genes

(A) The ratio of observed to expected number of DSB hotspots in the *dmc1*Δ strain (NKY1455) was calculated relative to the position of transcripts for four classes of regions: in genes or between tandem, divergent, or convergent transcripts. These data deviated significantly from those expected from a random distribution of the 258 hotspots in the single-copy genomic sequence (χ^2, $p = 7.4 \times 10^{-9}$).

(B) Composite ssDNA-enrichment profile. Array features associated with each gene were assigned to one of ten open reading frame (ORF) bins or five upstream or downstream intergenic bins on the basis of their relative position within each region. The profile represents the mean $\log_2$ ratios calculated for each bin.

(C) Heat map representing scaled $\log_2$ ratios of ssDNA enrichment for the upstream, coding, and downstream regions of each of the 226 largest genes coinciding with DSB sites in the *dmc1*Δ strain (NKY1455). For comparison across genes, mean $\log_2$ ratios for all features associated with each gene were adjusted to 0.

(D) The average expression level after 2 hr in sporulation media is shown for all genes (yellow bars) and the genes coinciding with DSB sites in the *dmc1*Δ strain (blue bars) for sporulating a/α and control nonsporulating α/α cells [28].

underrepresented at sites of convergent transcription and in coding regions (Figure 3A). To further refine the positions of break sites relative to genes, we calculated the composite ssDNA-enrichment profile for all 1105 genes overlapping a DSB hotspot. Consistent with the results above, the composite profile showed the highest ssDNA signal in the promoter region (Figure 3B). To resolve the position of break sites at individual genes, we plotted the relative ssDNA enrichment across the largest 226 hotspot-associated genes (Figure 3C). We found that ~80% of genes exhibited higher ssDNA signal in their promoters and 5′ ends relative to the rest of the coding or downstream regions. Moreover, the vast majority (44/47) of the 3′ regions that exhibited elevated ssDNA enrichment contained a promoter for the adjacent gene. Together, these findings are consistent with the model that the majority of DSBs occur in intergenic regions containing promoters.

Because the activity of a number of hotspots requires the binding of transcription factors [9, 19], we investigated the connection between transcription and DSB hotspots. By using published meiotic gene-expression data [28], we found that the average expression level of genes at peaks of DSB hotspots was 30% higher than the mean expression level in the genome (Student's t test, $p < 0.0009$; Figure 3D). However, we observed no enrichment of meiotically regulated genes within hotspots (Table S2). Similarly, there was no difference between expression levels of genes surrounding DSB hotspots from meiosis-competent *MATa/α* cells or meiosis-incompetent *MATα/α* cells (Figure 3D) [28]. These data imply that DSBs occur preferentially in the promoters of active, but not necessarily meiosis-specific, genes.

Strong Hotspots in the Pericentromeric Regions

Although recombination is repressed in pericentromeric regions, we detected a substantial number of meiotic DSB hotspots in the immediate vicinity of centromeres. Within a 50 kb window encompassing the cohesion-protected regions around the core centromeres [29], we observed as many DSB hotspots as expected from a model of random distribution (21 versus 17, Figure S3, blue triangles). We confirmed the existence of hotspots close to *CEN2*, *CEN4*, and *CEN15* by Southern blotting in both *dmc1*Δ and wild-type cells. In each case, one or several DSB hotspots could be detected within 5 kb of the centromere (inverted triangles, Figure 4 and Figure S4). We conclude that the pericentromeric regions are not protected from meiotic DSB formation.

Hotspot Distribution near the rDNA and Telomeres

We next analyzed DSB formation around the rDNA and near telomeres, genomic regions that were previously reported to exhibit a significantly lower than average number of DSB hotspots [10, 17–19, 30]. ssDNA analysis confirmed an absence of strong hotspots within 100 kb of the rDNA (chromosome XII; Figure S1). We also observed a depletion of hotspots within 20 kb of telomeres; in these regions, we detected only half the number of DSB hotspots expected from a random distribution model (6 versus 14, Figure 5A), and the mean distance from a telomere to the closest hotspot was 40 kb. Furthermore, when we plotted ssDNA enrichment versus distance from telomere for all data points, we observed a noticeable decrease in overall ssDNA enrichment in the first 20 kb from the telomere (Figure 5B). The 20 kb zone of DSB depletion is much more limited than that of previous studies involving *rad50S* or *sae2*Δ mutations that observed depletion of hotspots within 40–100 kb of telomeres [10, 17, 18, 30]. In our analysis of Spo11-binding sites, DSB hotspots were depleted within 40 kb of telomeres, and the mean distance from the telomere to the closest hotspot was 100 kb. We believe that the bias against telomere-proximal hotspots in the Spo11 ChIP experiments is due to the use of the *rad50S* background. Pulsed-field gel analysis revealed a selective reduction of DSBs near the left telomere of chromosome VIII in *rad50S* mutants (Figure 2B), and similar reduction was also observed for telomere-proximal hotspots on chromosome III [22]. The limited 20 kb zone of DSB depletion is supported by both

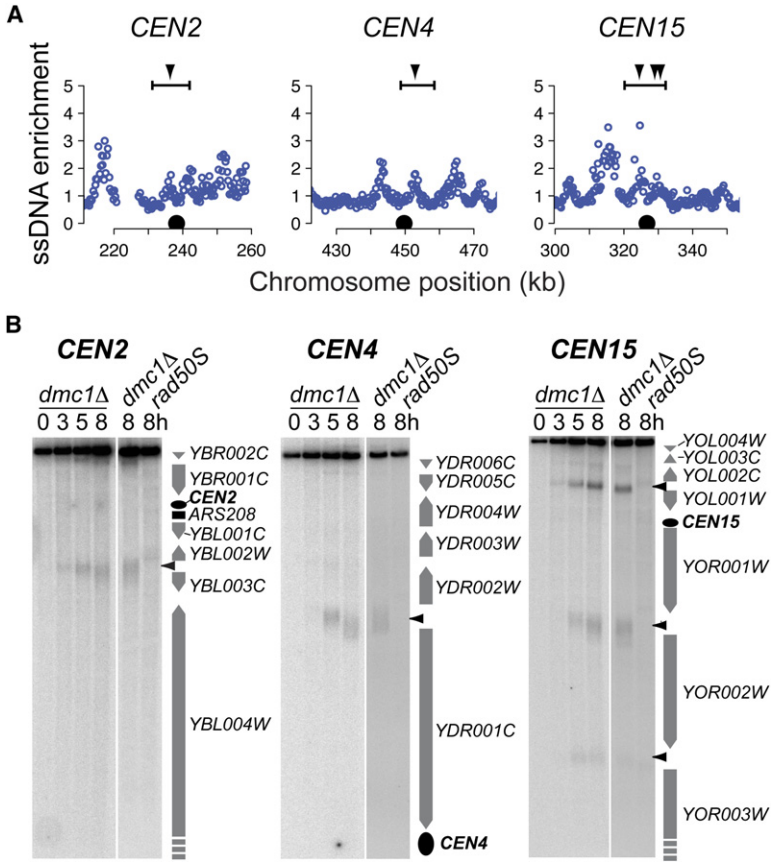

Figure 4. Hotspots near Centromeres

(A) ssDNA enrichment versus chromosome position is plotted for a window of ±25 kb for *CEN2*, *CEN4*, and *CEN15*. Black dots indicate the centromere position. Black bars indicate positions of restriction fragments detected by Southern blotting, and inverted triangles indicate confirmed DSB sites (see [B]).

(B) *dmc1*Δ (NKY1455) and *rad50S* (A11675) cells were induced to undergo synchronous meiosis. At the indicated time points, samples were collected, and DNA was analyzed by Southern blotting. The following restriction enzymes and probes (SGD coordinates) were used: *CEN2*, SacI, II:231,552-232,350; *CEN4*, SpeI, IV:449,212-449,721; and *CEN15*, SphI/NheI, XV:331,713-332,402. Gray arrows indicate the positions of open reading frames; black ovals indicate centromeres; and black arrowheads indicate major DSB sites.

genetic and microarray data that demonstrate a strong reduction of crossover recombination within 25–30 kb of telomeres [13] (J. Fung, personal communication).

Strikingly, in the region 20–120 kb from a telomere, hotpots mapped by ssDNA analysis were twice as prevalent as expected under a random distribution model (137 versus 68). Southern-blot analysis confirmed the existence of telomere-proximal hotspots on the left arm of chromosome XVI and on the right arm of chromosome III (*YPL274W*, *YPL255W*, *YPL221W*, *YCR024C-A*; Figure 2A and data not shown). By contrast, hotspots were underrepresented at distances >120 kb from a telomere; in these regions, we detected 115 hotspots instead of the expected 176. A similar trend of telomere-proximal enrichment and internal depletion of ssDNA was also observed when we plotted the total ssDNA signal versus distance from telomere for all data points (Figure 5C, blue points). The existence of elevated break levels close to the ends of chromosomes is supported by recent genetic data in yeast (D. Kaback, A. Barton, and J. Fung, personal communications).

The telomere-proximal enrichment of ssDNA might underlie a well-known and widely conserved meiotic phenomenon. Work from a number of organisms has shown that small chromosomes receive more crossovers per unit length than large chromosomes [31–33]. This bias might ensure that small chromosomes receive at least one crossover and are thus faithfully segregated during meiosis I. It has been suggested that this size bias is controlled, at least partially, at the level of DSBs, because analysis of Spo11 distribution indicated that small chromosomes had more hotspots per unit length and that these hotspots were "hotter" [10]. ssDNA-enrichment analysis similarly revealed that the average amount of ssDNA was higher for the smallest chromosomes (Figure 6A). Additionally, the two smallest chromosomes had far more hotspots per unit length as compared to the larger chromosomes (11 and 15 hotspots each, versus the expected five and six, respectively), although this bias did not extend to the other small chromosomes. Remarkably, when we plotted ssDNA enrichment for individual chromosomes, large and small chromosomes alike followed the same pattern of increased levels of DSBs within a 100 kb region near the chromosome ends (Figure 5C, lines). The 20–120 kb window size of increased ssDNA signal was constant for all chromosomes and is almost exactly half the size of the smallest chromosome (230 kb). Thus, the telomere-proximal enrichment of ssDNA probably accounts for the increased average ssDNA signal of small chromosomes (Figure 6A) and might ensure that all chromosomes receive sufficient DSBs, regardless of their size.

The observation that the DSB-enriched regions were present near the ends of all chromosomes raised the possibility that the proximity to telomeres induced higher DSB levels in these regions. Alternatively, subtle differences in local DNA sequence composition could lead to elevated DSB formation. To distinguish between these possibilities, we introduced new telomeres into a DSB-poor internal region by bisecting the right arm of chromosome XV. Strikingly, whereas there was no change in DSB levels immediately next to the new

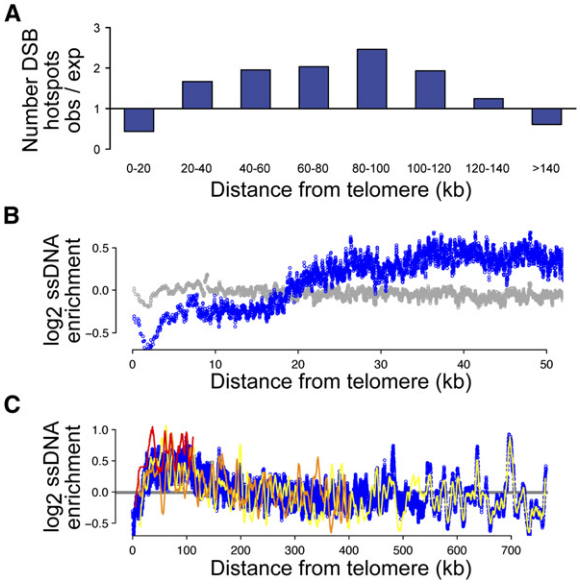

Figure 5. Levels of DSB Formation in Telomere-Proximal Regions

(A) The ratio of observed to expected number of DSB hotspot peaks in *dmc1*Δ (NKY1455) is plotted as a function of distance from the telomere. These data deviated significantly from those expected from a random distribution of the 258 hotspots in the single-copy genomic sequence (χ^2, p = 1.4 × 10^{-19}). Distance from telomere was defined from the start of annotated single-copy sequence at chromosome ends (SGD; www.yeastgenome.org).

(B) The $\log_2$ ratio of ssDNA-enrichment signal from all 32 subtelomeric regions was plotted as a function of distance from the telomere for *dmc1*Δ (NKY1455; blue) and *spo11-Y135F* (A10914; gray). Data were smoothed by application of a moving average over 20 consecutive points.

(C) As in (B), except the entire data set for all distances from telomere is shown for *dmc1*Δ (NKY1455; blue). The data points for the individual chromosomes I (red line), II (orange line), and IV (yellow line), smoothed by application of a moving average over 40 consecutive points, are overlaid on the total data profile.

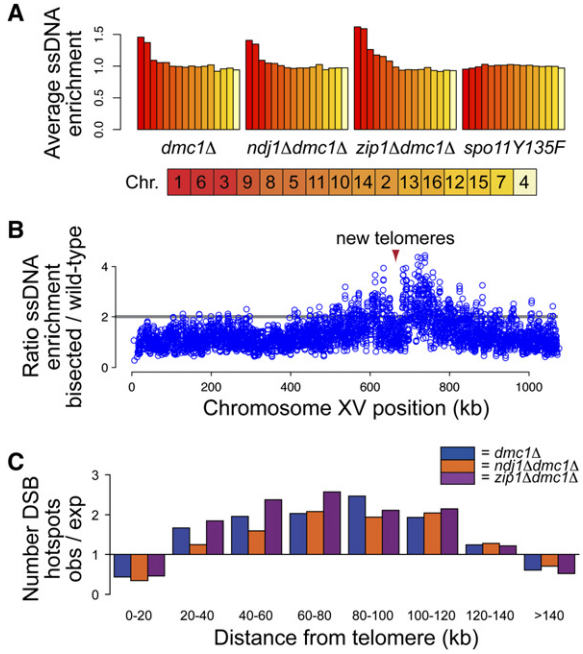

Figure 6. Effects of Telomeres on DSB Levels

(A) Average ssDNA enrichment per chromosome in *dmc1*Δ (NKY1455), *ndj1*Δ *dmc1*Δ (YAH2626), *zip1*Δ *dmc1*Δ (YAH2650), and *spo11-Y135F* (A10914) cells. The mean ssDNA-enrichment signal relative to the mean signal for the entire data set was calculated for all features on each chromosome. For chromosome XII, only the non-rDNA sequences were included in the analysis. Bars representing the normalized average ssDNA enrichment for each chromosome were sorted by chromosome length. Gradient colors correlate with chromosome length.

(B) The ratio of ssDNA enrichment was calculated for a *dmc1*Δ strain containing a bisected chromosome XV (YAH3112) relative to the wild-type chromosome XV *dmc1*Δ strain (NKY1455). The ratio of ssDNA enrichment (YAH3112/NKY1455) was plotted for chromosome XV. The average ssDNA-enrichment ratio of the two strains is 1. The arrowhead indicates the position where the chromosome was bisected, ~674 kb.

(C) The ratio of observed to expected number of DSB hotspot peaks is plotted as a function of distance from the telomere for *dmc1*Δ (NKY1455; blue), *ndj1*Δ *dmc1*Δ (YAH2626; orange), and *zip1*Δ *dmc1*Δ (YAH2650; purple). These data deviated significantly from those expected from a random distribution of the 258 hotspots in the single-copy genomic sequence (χ^2, p = 1.4 × 10^{-19}, 4.0 × 10^{-13}, and 2.0 × 10^{-31}, respectively).

telomeres, we found a marked increase in DSB levels within ~20–120 kb from the new chromosome ends (Figure 6B). We conclude that telomeres are sufficient to induce the 100 kb domain of DSB enrichment near chromosome ends.

During meiosis, chromosomes undergo major structural changes that might directly influence large-scale DSB distribution. Around the time of DSB formation, meiotic telomeres congress into a loose cluster conformation known as the bouquet [34]. The bouquet later disperses, and chromosomes become associated with the highly structured protein lattice of the synaptonemal complex (SC) [35]. To test whether bouquet formation or the SC affect large-scale DSB distribution, we analyzed the requirement for two factors: Ndj1, a telomeric protein necessary for bouquet formation [36–38], and Zip1, a central component of the SC that also plays a role in maintaining crossover interference [2, 39, 40]. Disruption of *NDJ1* had no apparent effect on DSB hotspot distribution (Figure S1). Like *dmc1*Δ cells, *ndj1*Δ *dmc1*Δ mutants demonstrated a biased hotspot distribution, with depletion in a 20 kb window near telomeres and enrichment outside that zone (Figure 6C). Furthermore, small chromosomes still exhibited increased ssDNA signal in *ndj1*Δ *dmc1*Δ mutants (Figure 6A). Similarly, deletion of *ZIP1* had no clear effect on hotspot distribution or the depletion of DSBs within 20 kb of telomeres (Figure S1 and Figure 6C), although we did notice a slight increase in the DSB signal of small chromosomes in *zip1*Δ *dmc1*Δ mutants (Figure 6A). We conclude that the telomere-proximal distribution of DSBs is predominantly independent of bouquet formation and the SC.

Discussion

In this study, we present a method for detecting DSB-associated ssDNA that can reliably predict DSB hotspots in both wild-type and mutant cells. Remarkably, we observed substantial DSB formation within the pericentromeric regions. Because interhomolog repair is suppressed around centromeres, our findings indicate a specialized mode of DSB repair in those regions. In

addition, analysis of ssDNA profiles revealed that telomeres induce elevated levels of DSBs within a broad zone from 20–120 kb from chromosome ends. This distribution of DSBs suggests a mechanism for ensuring that chromosomes of all sizes receive a minimum number of DSBs.

ssDNA-derived hotspot profiles differ noticeably from the profiles obtained by mapping Spo11-associated DNA. We believe that this difference is a consequence of the *rad50S*-type mutations used to trap Spo11 at DSB sites because these mutations alter the pattern of meiotic DSB formation [20–22]. Although not all hotspots are affected, we demonstrate that many DSB hotspots close to telomeres and centromeres are substantially less active in *rad50S* mutants. At this point, it is unclear why only some hotspots are sensitive to *rad50S*-type mutations. The fact that *rad50S* is epistatic to *dmc1*Δ with respect to DSB distribution argues against the possibility that DSBs at *rad50S*-sensitive hotspots are turned over more rapidly [20]. Rather, it appears that these breaks never form. It is possible that feedback mechanisms halt DSB formation as aberrant DSBs accumulate in *rad50S* mutants. Alternatively, there could be limiting levels of factors that are not recycled when Spo11 is not released. In either case, one would predict that *rad50S*-sensitive hotspots form DSBs later than hotspots not affected by this mutation.

Remarkably, we found that DSB levels around centromeres are much higher than predicted from the low rates of meiotic recombination in these regions. For example, quantification of the Southern signal at the *YDR001C* hotspot (Figure 4B, middle panel), indicated that 7.8% ± 1.8% of chromosomes receive a DSB at this site. *YDR001C* lies between *CEN4* and the well-characterized centromere-linked marker *TRP1* (*YDR007W*). Assuming that *YDR001C* is the only major hotspot between these two markers, we would expect a genetic distance between *CEN4* and *TRP1* of ~7.5 cM (see Supplemental Data), substantially more than the 0.3–0.5 cM observed in mapping studies (www.yeastgenome.org). Therefore, crossover repair can only account for approximately 5% of repair at *YDR001C*. Interestingly, repair from the homolog without strand exchange (noncrossover repair) is thought to be similarly reduced in pericentromeric regions [41]. These data strongly suggest that centromeric DSBs are less frequently repaired by homolog-directed DSB repair than breaks in other parts of the genome.

Our results indicate that an alternate pathway governs DSB repair around centromeres. The fact that centromeric DSBs accumulate in the absence of the Dmc1 recombinase argues that these breaks are not repaired by nonhomologous end joining, but rather by homologous recombination. Because Dmc1 is required for both meiotic interhomolog and intersister repair [27], we favor the possibility that pericentromeric DSBs are repaired with the sister chromatid as the preferred repair template. Intersister repair normally accounts for only ~20% of the DSB repair events during meiotic recombination [27, 42]. However, meiotic DSBs within the repetitive rDNA array are almost exclusively repaired from the sister chromatid [43]. A similar meiotic intersister repair bias might exist around centromeres. Interestingly, the abundance of Red1, a lateral element component that prevents meiotic intersister repair, is selectively reduced near *CEN3* [21]. It is tempting to speculate that local depletion of Red1 allows intersister repair around centromeres. Alternatively, the high concentration of cohesin complexes at centromeres or a distinct subunit composition of centromeric cohesin complexes, as observed in *S. pombe* [44], could also influence DSB repair in the pericentromeric regions.

The distribution of meiotic DSB hotspots is regulated on multiple levels. Locally, DSBs are known to occur almost exclusively in intergenic regions containing promoters, although not all promoter regions receive DSBs [9, 15, 16]. Our results point to a role of transcriptional activation in promoting DSB formation because we observed an enrichment of highly expressed genes at hotspots. However, studies of the *HIS4*-associated hotspot suggest that it might not be transcription of these genes per se that is necessary for hotspot activity [45]. Instead, transcription factors and histone modifications associated with transcriptional activation might contribute to a chromatin environment that provides accessibility to DSB factors [9, 46]. High GC content was also implicated in the regulation of DSB formation [10, 19, 47]. We found that the GC content of intergenic regions containing DSB hotspots was higher than average (37.87% versus 35.35%, Student's t test, $p = 2.2 \times 10^{-16}$). However, this correlation could be driven, at least in part, by the fact that DSB hotspots are overrepresented in promoter-containing and larger intergenic regions, both of which have higher than average GC content.

In addition to local regulation, DSB formation is also controlled regionally, in particular near chromosome ends. We observed two very defined regions near telomeres; the distal-most ~20 kb of single-copy sequence were predominantly devoid of hotspots, whereas the next ~100 kb exhibited higher levels of DSB formation than the rest of the genome. How might this DSB distribution be regulated? The depletion of DSBs within 20 kb of telomeres might be, at least partially, a *cis* effect of the repeat-rich DNA sequences found in immediate proximity of yeast subtelomeric regions because recombination remains low when these sequences are moved to more internal positions [48]. By contrast, we could induce DSB-rich 100 kb regions ectopically on chromosome XV by introducing new telomeres. This effect argues against a role of the local DNA sequence in establishing the 100 kb regions and would be consistent with the spreading of a *trans*-acting factor from chromosome ends. Sir-dependent heterochromatin has been reported to affect 4–16 kb of single-copy sequence at chromosome ends [49] and might control DSB formation. Interestingly, deletion of the *SIR2* gene not only leads to an increase in DSBs near telomeres but also to a decrease in DSB formation within 10–120 kb from the telomeres [30], a region that is very similar to the domain in which we observe increased DSB activity. It might be worth using ssDNA enrichment to investigate the role of telomeric heterochromatin in regulating DSB activity because this method provides increased sensitivity in detection of telomere-proximal DSBs. Finally, although we have excluded a role for bouquet formation or the SC, it remains a possibility that other aspects of nuclear architecture such as chromosomal position with respect to the nuclear periphery or the nucleolus might influence the regional distribution of DSBs.

Small chromosomes exhibit higher relative levels of crossover formation than large chromosomes [31–33]. We propose that this effect is driven, at least in part, by the telomere-induced increase in DSB formation near chromosome ends, which has a proportionally stronger influence on small chromosomes. A localized increase in DSB formation can also explain why a recent report analyzing genetic recombination on translocated chromosomes failed to find a chromosome-size effect. The analyzed telomere proximal intervals did not change their position with respect to the 100 kb domains [50]. Theoretical work has suggested the existence of two pathways that control crossover distribution [51]. The major pathway is under the control of crossover interference, a chromosome-size-dependent mechanism that functions to distribute crossovers evenly along chromosomes. In addition, that study postulated a minor interference-independent pathway that leads to roughly equal amounts of crossovers on all chromosomes, independent of their size [51]. Because the telomere-proximal domains lead to a chromosome-size-independent increase in DSB formation, we speculate that these domains function in such an interference-independent pathway of crossover formation. In this respect, our observation that *zip1*Δ *dmc1*Δ mutants exhibit somewhat increased levels of DSB formation on small chromosomes is interesting, because disruption of *MSH4*, which acts in the same epistasis group as *ZIP1* [52], leads to an increase in crossover recombination specifically on small chromosomes [51]. This observation raises the possibility that the increase in recombination in *msh4* mutants occurs at the level of DSB formation and supports the idea that the DSB-enriched domains near telomeres function in the interference-independent pathway of crossover formation.

In humans, average recombination rates of small chromosomes are approximately twice as high as those of large chromosomes [31]. It is possible that similar regions of increased DSB formation exist near the ends of human chromosomes. Because ssDNA is thought to be a universal intermediate of homologous recombination, adaptations of the method presented here should permit the mapping and analysis of meiotic DSB hotspots in other eukaryotes, including mice and humans.

Experimental Procedures

ssDNA Isolation

ssDNA isolation was based on a method described in [53]. For each time point, $\sim 10^9$ cells were fixed in 70% ethanol at −20°C. Cells were spheroplasted in sorbitol buffer (1 M sorbitol, 1% beta-mercaptoethanol, 0.2 mg/ml zymolyase 100T, and 0.1M EDTA [pH 7.4]), lysed in NDS (0.6% SDS, 300 mM EDTA, 10 mM Tris-HCl [pH 9.5]). DNA was deproteinated with proteinase K (0.25 mg/ml; Roche) at 50°C, twice phenol extracted, treated with RNase A, and stored in TE (1 mM EDTA, 10 mM Tris-HCl [pH 7.5]) at 4°C. A total of 25 μg DNA were digested to completion with EcoRI (New England Biolabs). ssDNA was enriched by batch absorption to BND cellulose as previously described [54]. In brief, a 50% slurry of BND-cellulose was equilibrated in NET (1 M NaCl, 10 mM Tris [pH 7.6], and 1 mM EDTA). Digested DNA was adjusted to 1 M NaCl, and ssDNA was incubated with a 500 μl bed volume of BND-cellulose for 5 min. Resin was washed with five bed volumes of NET. ssDNA was eluted five times with 600 μl NET + 1.8% caffeine. DNA was precipitated and concentrated for microarray analysis.

Microarray Detection of ssDNA

A total of 1.5 μg each of 0 hr and 3 or 5 hr ssDNA samples were labeled with Cy3-dUTP or Cy5-dUTP (GE Healthcare) by random priming without denaturation with 4 μg random nonamer oligo (Integrated DNA Technologies) and 10 units of Klenow (New England Biolabs). Unincorporated dye was removed with microcon columns (30 kDa MW cutoff; Millipore), and samples were cohybridized to custom Agilent arrays in accordance with a standard protocol. For each set of experiments, a dye swap was performed.

Microarray-Data Analysis

For each cohybridization, Cy3 and Cy5 levels were calculated with Agilent Feature Extractor CGH software. Background normalization, $\log_2$ ratios for each experiment, and scale normalizations across each set of duplicated experiments were calculated with the sma package [55] in R, a computer language and environment for statistical computing (v2.1.0, http://www.r-project.org). DSB sites were defined as >3 points within 500 bp of each other on the same chromosome that all had p values < 0.125 (using pnorm function in R) in each of two independent experiments. The DSB site was defined as a merged region from start to end of all significant data points. The peak was plotted at the location of the maximum ssDNA signal after smoothing by application of a moving average across five consecutive chromosomal features. For peak comparisons within high-density data sets, DSB sites were defined as the same if any of the enriched points were identical.

Supplemental Data

Additional Experimental Procedures, four figures, and two tables are available at http://www.current-biology.com/cgi/content/full/17/23/2003/DC1/.

Acknowledgments

We are grateful to N. Kleckner, A. Amon, and F. Klein for providing strains. We thank J. Falk for technical assistance and M. de Vries, A. Amon, and T. Orr-Weaver for helpful discussions and critical reading of the manuscript. We are indebted to M. Lichten, J. Fung, A. Barton, and D. Kaback for sharing data prior to publication. S.P.B. is an investigator of the Howard Hughes Medical Institute.

Received: July 31, 2007
Revised: October 10, 2007
Accepted: October 23, 2007
Published online: November 29, 2007

References

1. Petronczki, M., Siomos, M.F., and Nasmyth, K. (2003). Un menage a quatre: The molecular biology of chromosome segregation in meiosis. Cell *112*, 423–440.
2. Bishop, D.K., and Zickler, D. (2004). Early decision; meiotic crossover interference prior to stable strand exchange and synapsis. Cell *117*, 9–15.
3. Bergerat, A., de Massy, B., Gadelle, D., Varoutas, P.-C., Nicholas, A., and Forterre, P. (1997). An atypical topoisomerase II from Archaea with implications for meiotic recombination. Nature *386*, 414–417.
4. Keeney, S., Giroux, C.N., and Kleckner, N. (1997). Meiosis-specific DNA double-strand breaks are catalyzed by Spo11, a member of a widely conserved protein family. Cell *88*, 375–384.
5. Sun, H., Treco, D., and Szostak, J.W. (1991). Extensive 3′-overhanging, single-stranded DNA associated with the meiosis-specific double-strand breaks at the ARG4 recombination initiation site. Cell *64*, 1155–1161.
6. Allers, T., and Lichten, M. (2001). Differential timing and control of noncrossover and crossover recombination during meiosis. Cell *106*, 47–57.
7. Hunter, N., and Kleckner, N. (2001). The single-end invasion: An asymmetric intermediate at the double-strand break to double-holliday junction transition of meiotic recombination. Cell *106*, 59–70.

8. Lichten, M., and Goldman, A.S. (1995). Meiotic recombination hotspots. Annu. Rev. Genet. *29*, 423–444.
9. Petes, T.D. (2001). Meiotic recombination hot spots and cold spots. Nat. Rev. Genet. *2*, 360–369.
10. Gerton, J.L., DeRisi, J., Shroff, R., Lichten, M., Brown, P.O., and Petes, T.D. (2000). Inaugural article: Global mapping of meiotic recombination hotspots and coldspots in the yeast Saccharomyces cerevisiae. Proc. Natl. Acad. Sci. USA *97*, 11383–11390.
11. Rockmill, B., Voelkel-Meiman, K., and Roeder, G.S. (2006). Centromere-proximal crossovers are associated with precocious separation of sister chromatids during meiosis in Saccharomyces cerevisiae. Genetics *174*, 1745–1754.
12. Lamb, N.E., Sherman, S.L., and Hassold, T.J. (2005). Effect of meiotic recombination on the production of aneuploid gametes in humans. Cytogenet. Genome Res. *111*, 250–255.
13. Su, Y., Barton, A.B., and Kaback, D.B. (2000). Decreased meiotic reciprocal recombination in subtelomeric regions in Saccharomyces cerevisiae. Chromosoma *109*, 467–475.
14. Petes, T.D., and Botstein, D. (1977). Simple Mendelian inheritance of the reiterated ribosomal DNA of yeast. Proc. Natl. Acad. Sci. USA *74*, 5091–5095.
15. Wu, T.C., and Lichten, M. (1994). Meiosis-induced double-strand break sites determined by yeast chromatin structure. Science *263*, 515–518.
16. Baudat, F., and Nicolas, A. (1997). Clustering of meiotic double-strand breaks on yeast chromosome III. Proc. Natl. Acad. Sci. USA *94*, 5213–5218.
17. Borde, V., Lin, W., Novikov, E., Petrini, J.H., Lichten, M., and Nicolas, A. (2004). Association of Mre11p with double-strand break sites during yeast meiosis. Mol. Cell *13*, 389–401.
18. Robine, N., Uematsu, N., Amiot, F., Gidrol, X., Barillot, E., Nicolas, A., and Borde, V. (2007). Genome-wide redistribution of meiotic double-strand breaks in Saccharomyces cerevisiae. Mol. Cell. Biol. *27*, 1868–1880.
19. Mieczkowski, P.A., Dominska, M., Buck, M.J., Gerton, J.L., Lieb, J.D., and Petes, T.D. (2006). Global analysis of the relationship between the binding of the Bas1p transcription factor and meiosis-specific double-strand DNA breaks in Saccharomyces cerevisiae. Mol. Cell. Biol. *26*, 1014–1027.
20. Dresser, M.E., Ewing, D.J., Conrad, M.N., Dominguez, A.M., Barstead, R., Jiang, H., and Kodadek, T. (1997). DMC1 functions in a Saccharomyces cerevisiae meiotic pathway that is largely independent of the RAD51 pathway. Genetics *147*, 533–544.
21. Blat, Y., Protacio, R.U., Hunter, N., and Kleckner, N. (2002). Physical and functional interactions among basic chromosome organizational features govern early steps of meiotic chiasma formation. Cell *111*, 791–802.
22. Borde, V., Goldman, A.S.H., and Lichten, M. (2000). Direct coupling between meiotic DNA replication and recombination initiation. Science *290*, 806–809.
23. Cao, L., Alani, E., and Kleckner, N. (1990). A pathway for generation and processing of double-strand breaks during meiotic recombination in S. cerevisiae. Cell *61*, 1089–1101.
24. Feng, W., Collingwood, D., Boeck, M.E., Fox, L.A., Alvino, G.M., Fangman, W.L., Raghuraman, M.K., and Brewer, B.J. (2006). Genomic mapping of single-stranded DNA in hydroxyurea-challenged yeasts identifies origins of replication. Nat. Cell Biol. *8*, 148–155.
25. Bishop, D.K., Park, D., Xu, L., and Kleckner, N. (1992). DMC1: A meiosis-specific yeast homolog of E. coli recA required for recombination, synaptonemal complex formation, and cell cycle progression. Cell *69*, 439–456.
26. Buhler, C., Borde, V., and Lichten, M. (2007). Mapping meiotic single-strand DNA reveals a new landscape of DNA double strand breaks in Saccharomyces cerevisiae. PLoS Biol. *5*, e324.
27. Schwacha, A., and Kleckner, N. (1997). Interhomolog bias during meiotic recombination: Meiotic functions promote a highly differentiated interhomolog-only pathway. Cell *90*, 1123–1135.
28. Primig, M., Williams, R.M., Winzeler, E.A., Tevzadze, G.G., Conway, A.R., Hwang, S.Y., Davis, R.W., and Esposito, R.E. (2000). The core meiotic transcriptome in budding yeasts. Nat. Genet. *26*, 415–423.
29. Kiburz, B.M., Reynolds, D.B., Megee, P.C., Marston, A.L., Lee, B.H., Lee, T.I., Levine, S.S., Young, R.A., and Amon, A. (2005). The core centromere and Sgo1 establish a 50-kb cohesin-protected domain around centromeres during meiosis I. Genes Dev. *19*, 3017–3030.
30. Mieczkowski, P.A., Dominska, M., Buck, M.J., Lieb, J.D., and Petes, T.D. (2007). Loss of a histone deacetylase dramatically alters the genomic distribution of Spo11p-catalyzed DNA breaks in Saccharomyces cerevisiae. Proc. Natl. Acad. Sci. USA *104*, 3955–3960.
31. Kong, A., Gudbjartsson, D.F., Sainz, J., Jonsdottir, G.M., Gudjonsson, S.A., Richardsson, B., Sigurdardottir, S., Barnard, J., Hallbeck, B., Masson, G., et al. (2002). A high-resolution recombination map of the human genome. Nat. Genet. *31*, 241–247.
32. Kaback, D.B., Guacci, V., Barber, D., and Mahon, J.W. (1992). Chromosome size-dependent control of meiotic recombination. Science *256*, 228–232.
33. Copenhaver, G.P., Browne, W.E., and Preuss, D. (1998). Assaying genome-wide recombination and centromere functions with Arabidopsis tetrads. Proc. Natl. Acad. Sci. USA *95*, 247–252.
34. Scherthan, H. (2001). A bouquet makes ends meet. Nat. Rev. Mol. Cell Biol. *2*, 621–627.
35. Zickler, D. (2006). From early homologue recognition to synaptonemal complex formation. Chromosoma *115*, 158–174.
36. Chua, P.R., and Roeder, G.S. (1997). Tam1, a telomere-associated meiotic protein, functions in chromosome synapsis and crossover interference. Genes Dev. *11*, 1786–1800.
37. Conrad, M.N., Dominguez, A.M., and Dresser, M.E. (1997). Ndj1p, a meiotic telomere protein required for normal chromosome synapsis and segregation in yeast. Science *276*, 1252–1255.
38. Trelles-Sticken, E., Dresser, M.E., and Scherthan, H. (2000). Meiotic telomere protein Ndj1 is required for meiosis-specific telomere distribution, bouquet formation, and efficient homolog pairing. J. Cell Biol. *151*, 95–106.
39. Sym, M., Engebrecht, J.A., and Roeder, G.S. (1993). ZIP1 is a synaptonemal complex protein required for meiotic chromosome synapsis. Cell *72*, 365–378.
40. Sym, M., and Roeder, G.S. (1994). Crossover interference is abolished in the absence of a synaptonemal complex protein. Cell *79*, 283–292.
41. Lambie, E.J., and Roeder, G.S. (1988). A yeast centromere acts in cis to inhibit meiotic gene conversion of adjacent sequences. Cell *52*, 863–873.
42. Haber, J.E., Thorburn, P.C., and Rogers, D. (1984). Meiotic and mitotic behavior of dicentric chromosomes in Saccharomyces cerevisiae. Genetics *106*, 185–205.
43. Petes, T.D., and Pukkila, P.J. (1995). Meiotic sister chromatid recombination. Adv. Genet. *33*, 41–62.
44. Kitajima, T.S., Yokobayashi, S., Yamamoto, M., and Watanabe, Y. (2003). Distinct cohesin complexes organize meiotic chromosome domains. Science *300*, 1152–1155.
45. White, M.A., Dominska, M., and Petes, T.D. (1993). Transcription factors are required for the meiotic recombination hotspot at the HIS4 locus in Saccharomyces cerevisiae. Proc. Natl. Acad. Sci. USA *90*, 6621–6625.
46. Maleki, S., and Keeney, S. (2004). Modifying histones and initiating meiotic recombination; new answers to an old question. Cell *118*, 404–406.
47. Birdsell, J.A. (2002). Integrating genomics, bioinformatics, and classical genetics to study the effects of recombination on genome evolution. Mol. Biol. Evol. *19*, 1181–1197.
48. Barton, A.B., Su, Y., Lamb, J., Barber, D., and Kaback, D.B. (2003). A function for subtelomeric DNA in Saccharomyces cerevisiae. Genetics *165*, 929–934.
49. Renauld, H., Aparicio, O.M., Zierath, P.D., Billington, B.L., Chhablani, S.K., and Gottschling, D.E. (1993). Silent domains are assembled continuously from the telomere and are defined by promoter distance and strength, and by SIR3 dosage. Genes Dev. *7*, 1133–1145.
50. Turney, D., de Los Santos, T., and Hollingsworth, N.M. (2004). Does chromosome size affect map distance and genetic interference in budding yeast? Genetics *168*, 2421–2424.

51. Stahl, F.W., Foss, H.M., Young, L.S., Borts, R.H., Abdullah, M.F., and Copenhaver, G.P. (2004). Does crossover interference count in Saccharomyces cerevisiae? Genetics *168*, 35–48.
52. Borner, G.V., Kleckner, N., and Hunter, N. (2004). Crossover/noncrossover differentiation, synaptonemal complex formation, and regulatory surveillance at the leptotene/zygotene transition of meiosis. Cell *117*, 29–45.
53. MacAlpine, D.M., Perlman, P.S., and Butow, R.A. (1998). The high mobility group protein Abf2p influences the level of yeast mitochondrial DNA recombination intermediates in vivo. Proc. Natl. Acad. Sci. USA *95*, 6739–6743.
54. Huberman, J.A., Spotila, L.D., Nawotka, K.A., el-Assouli, S.M., and Davis, L.R. (1987). The in vivo replication origin of the yeast 2 microns plasmid. Cell *51*, 473–481.
55. Yang, Y.H., Dudoit, S., Luu, P., and Speed, T.P. (2002). Normalization for cDNA microarray data: A robust composite method addressing single and multiple slide systematic variation. Nucleic Acids Res. *30*, e15.

Accession Numbers

All data sets in this publication have been deposited in the NCBI Gene Expression Omnibus (http://www.ncbi.nlm.nih.gov/geo/) and are accessible through GEO Series accession number GSE9503.